Available online at www.sciencedirect.com
ScienceDirect
Developmental Biology 298 (2006) 514–526
DEVELOPMENTAL BIOLOGY
www.elsevier.com/locate/ydbio

Noggin1 and Follistatin-like2 function redundantly to Chordin to antagonize BMP activity

Sophie Dal-Pra [1], Maximilian Fürthauer [1], Jeanne Van-Celst, Bernard Thisse, Christine Thisse *

Institut de Génétique et de Biologie Moléculaire et Cellulaire, UMR 7104, CNRS/INSERM/ULP, 1 rue Laurent Fries, BP 10142, CU de Strasbourg, 67404 ILLKIRCH Cedex, France

Received for publication 12 March 2006; revised 6 July 2006; accepted 7 July 2006
Available online 12 July 2006

Abstract

In *Xenopus*, the dorso-ventral (D/V) axis is thought to be specified by the bone morphogenetic proteins (Bmp) activity arising through interaction with antagonists such as Noggin, Chordin and Follistatin. We report here, through inactivation of *noggin1* (*nog1*) that this gene is not essential by itself to establish the D/V patterning. However, at blastula stage, inactivation of *nog1* strongly amplifies *chordin* (*chd*) phenotype, revealing redundant functions of these two genes on D/V axis formation. Substantial dorsal tissues remaining in the double *nog1-chd* morphant suggested that other anti-Bmp factors may pattern the D/V axis. We isolated two potential candidates, the *follistatin-like* (*fstl*) genes. We found that *fstl2* is an early gastrula expressed gene. Its inactivation, similar to *nog1*, strongly enhances the *chd* phenotype. Moreover, the penetrance of the ventralization phenotype is much higher when we inactivated simultaneously *chd*, *nog1* and *fstl2*.

Altogether, our data reveal that, while Chordin is the main player of the D/V axis, sufficient to maintain proper activity of Bmp gradient, the structures remaining in the *chd* mutant (namely dorsal and dorso-lateral territories, in both mesodermal and ectodermal layers) result from the anti-Bmp activity carried by Nog1 and Fstl2 at blastula and gastrula stages.

Keywords: Zebrafish; Gastrulation; Dorso-ventral axis; *BMP*; *noggin*; *chordin*; *ogon*; *follistatin*; *follistatin-like*

Introduction

The dorso-ventral axis of the *Xenopus* embryo is thought to be specified by a gradient of bone morphogenetic proteins activity that in part arises through the interaction with antagonists emanating from the dorsal organizer, Noggin, Chordin and Follistatin. These three factors bind to Bmps preventing them to activate their receptors, thereby blocking Bmp ventralizing properties (Piccolo et al., 1996; Zimmerman et al., 1996). Modulating this interaction is a metalloprotease Tolloid, which cleaves Chordin, allowing refining the limits of its activity *in vivo* (Marques et al., 1997; Piccolo et al., 1997; Connors et al., 1999). The key role for Bmp signaling in dorso-ventral (D/V) patterning was further supported by genetic analyses performed in the zebrafish and in the mouse models. To exemplify, in the zebrafish, dorsalized *swirl* mutants are altered in the *bmp2b* gene (Kishimoto et al., 1997; Nguyen et al., 1998) whereas the dorsalized *snailhouse* mutation is defective in the *bmp7* gene, revealing equivalent genetic roles for these two Bmp ligands (Schmid et al., 2000; Dick et al., 2000). Further analysis revealed that Bmp2b and Bmp7 synergize in a cell-autonomous mechanism, suggesting that Bmp2b/Bmp7 heterodimers act *in vivo* to specify ventral cell fates (Schmid et al., 2000).

Two additional mutations were identified within the course of zebrafish mutagenesis screens to produce ventralized phenotypes. The first mutation is *chordino* (*din*) that affects the *chordin* locus (Miller-Bertoglio et al., 1997; Schulte-Merker et al., 1997), and the second one is *ogon* (Hammerschmidt et al., 1996; Miller-Bertoglio et al., 1999), which codes for Sizzled, a member of the frizzled-related protein family (Martyn and Schulte-Merker, 2003; Yabe et al., 2003). The *Xenopus* homologue of Sizzled was recently shown to affect the D/V patterning through binding and inhibition of Tolloid. A similar activity for Sizzled in the zebrafish was recently described (Muraoka et al., 2006 and our unpublished observations).

* Corresponding author. Fax: +33 3 88 65 32 01.
E-mail address: thisse@igbmc.u-strasbg.fr (C. Thisse).
[1] These authors contributed equally to the work.

0012-1606/$ - see front matter © 2006 Elsevier Inc. All rights reserved.
doi:10.1016/j.ydbio.2006.07.002

Therefore, loss of Ogon upregulates Tolloid, resulting in an inactivation of Chordin (Lee et al., 2006; Muraoka et al., 2006).

While the *noggin* and *follistatin* genes were also identified in zebrafish, their implication in the establishment of the D/V patterning was far less clear because their possible implication on this process relied only on overexpression analyses (Bauer et al., 1998; Fürthauer et al., 1999). We isolated three *noggin* genes (Fürthauer et al., 1999), and two *follistatin* genes (Bauer et al., 1998 and this report) were found in the zebrafish genome. Gene expression analysis revealed that *noggin2*, *noggin3*, *follistatin1* and *follistatin2* are expressed too late during embryonic development to play a role in the establishment of the D/V patterning. On the other hand, *noggin1* is expressed at the dorsal blastula margin, making this factor a potential good candidate for its involvement in this process. In addition, we identified a novel member of the *follistatin* gene superfamily called *follistatin-like2* (*fstl2*), which is expressed in dorsal tissues at early gastrula stages, suggesting an implication of this factor in D/V patterning as well.

In the present study, we investigate the implication of *noggin1* and *follistatin-like2* in the establishment of the D/V patterning by loss of function experiments using the morpholino knock-down technology. Conversely to overexpression results, inactivation of *noggin1* has no effect on zebrafish D/V patterning. However, inactivation of *noggin1* together with *chordin* strongly enhances the ventralization phenotype observed after single loss of *chordin*. Similar results are obtained with *follistatin-like2*. Moreover, triple inactivation of *noggin1*, *chordin* and *follistatin-like2* leads to extreme ventralization. Altogether, our results clearly show that Chordin, Noggin1 and Follistatin-like2 function redundantly to control the establishment of the D/V axis of the zebrafish embryo.

Materials and methods

Zebrafish mutations

The spontaneous mutation *ogo m60* (*ogo*) and *dino tm84* (*din*) were used (Hammerschmidt et al., 1996; Miller-Bertoglio et al., 1999).

Whole-mount in situ hybridizations

Whole-mount *in situ* hybridizations were performed as described by Thisse et al. (2004) using the following probes.

Probes for *sox19* (clone CB799), *starmaker* (clone CB885), *ved* (clone CB675), im:7144261, *cyp26a* (clone CB24), *foxi1* (clone CB724), *drl* (clone CB253), *myf5* (clone CB641), *fst1* (clone CB446) and *hgg1* (clone CB15) were prepared as described in Thisse et al. (2001) and Thisse et al. (2004).

The probes for *flh* were prepared as described in Talbot et al. (1995), for *nog1* as described in Fürthauer et al. (1999) and for *chd* as described in Schulte-Merker et al. (1997). For *ogon* an RT-PCR fragment containing the full ORF of *sizzled* was cloned into a TOPO vector and the antisense probe was synthesized after PCR amplification of the insert with the PU and RP primers using the T7 RNA polymerase.

For *fst2* (sequence accession number: DQ317969), a 3′UTR fragment was PCR-amplified and subcloned into the *Bam*HI/*Xho*I sites of pBSKII (+). For probe synthesis, the vector was linearized with *Bam*HI and antisense RNA synthesized using T7 RNA Polymerase.

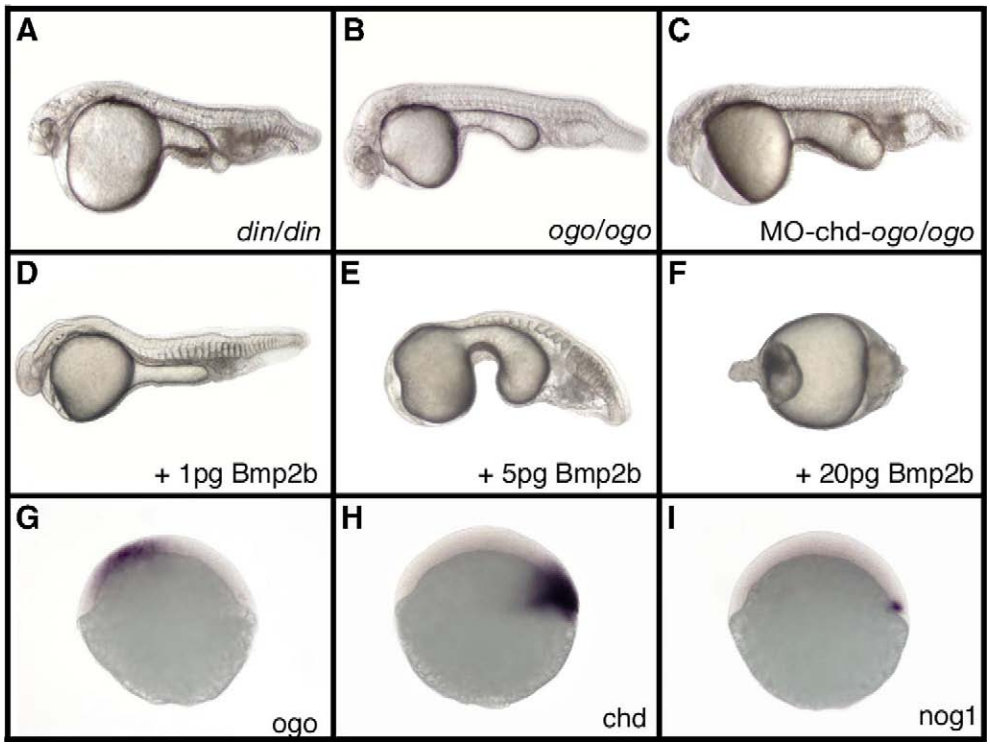

Fig. 1. Comparative analysis of ventralization phenotypes. Homozygous mutant embryos for *chordin* (*din*/*din*, panel A), *ogon* (*ogo*/*ogo*, panel B) as well as *chd* morphants in *ogon* mutant background (C) display ventralization phenotypes similar to those obtained after injection of low amount of *bmp2b* RNA (1 pg, panel D). Injection of 5 pg *bmp2b* RNA (E) results in stronger ventralization with complete loss of head while injection of 20 pg RNA (F) completely abolishes the D/V patterning and embryos appear radialized. At the onset of gastrulation, *ogo* transcripts (G) are observed in the ventral part of the embryo while *chd* (H) is expressed in a broad dorsal domain, which includes the *nog1* expression territory (I). Embryos are in lateral view, anterior to the left (A–F) or anterior to the top (G–I).

For *fstl1* (sequence accession number: DQ317970) a 1.5 kb fragment was inserted in the *Pst*I/*Xba*I sites of pBSKII (+). For probe synthesis, the template was linearized with *Pst*I and antisense RNA synthesized using T3 RNA polymerase.

For *fstl2* (sequence accession number: DQ317971), library screening led to the isolation of a 3 kb full-length cDNA inserted into the *Eco*RI/*Xho*I sites of pBSKII (+). For *in situ* hybridization, this vector was linearized with *Bam*HI and antisense RNA synthesized using T7 RNA polymerase to generate a 2 kb 3′UTR probe.

Injections

Morpholinos (Gene Tools) were resuspended in Danieau 1×, stored at −20°C as a 4 mM stock solution and diluted before use to the appropriate concentration. The sequences of the morpholinos used are:

morpholino chd:
MO-chd: ATCCACAGCAGCCCCTCCATCATCC
morpholinos noggin1:
MOa-nog1: GCGGGAAATCCATCCTTTTGAAATC covering the ATG of initiation of *nog1* translation
MOb-nog1: GAGATTAAACGCGGGATTTATCCGT located in the 5′ UTR, upstream of the *nog1* initiation codon
morpholinos follistatin1:
MOa-fst1: CTGACGCTTTAGCATCCTTAGCATG covering the *fst1* translation initiation site
MOb-fst1: GACGAGCAGCGCAAAAGTAATCTTC located in the 5′ UTR, upstream of the *fst1* initiation site
morpholinos follistatin-like 2:
MOa-fstl2: AAACACGGGTAAACACCGAAACATC covering the ATG of initiation of *fstl2* translation
MOb-fstl2: AAAAAACGCCGCCTGGGTGTCTGT located in the 5′ UTR, upstream of the *fstl2* initiation codon
morpholino ogon:
MO-ogo: ACAGCAGCAGACTGAATAGAGACAT.

For overexpression experiments, cDNAs (*fgf8*, *fst1* and *fstl2*) inserted into pCS2+ were linearized with *Not*I and transcribed using the SP6 RNA polymerase.

For mRNA and morpholino injections, embryos were dechorionated using Pronase E and injected with either RNA or morpholinos diluted in 0.2% Phenol Red and 0.1 M KCl, using an Eppendorf 5426 microinjector.

Phenotypic analyses

For morphological analysis, embryos were sorted out into 3 different classes according to their D/V axis defects and named C1 (ventralization similar to ventralization of *chd* loss of function), C2 (strong ventralization, with complete deletion of anterior head) and C3 (extreme ventralization—complete loss of head structures), while for the analysis after whole-mount *in situ* hybridization, embryos were sorted out into 2 different classes labeled CI (weak ventralization) and CII (strong ventralization) at early developmental stages and into 3 classes (CI to CIII from weak ventralization – CI – to extreme ventralization—CIII) at 30 hpf.

Fig. 2. *noggin1* morphants display normal D/V patterning. Compared to wild-type at 30 hpf (A), MO-nog1-injected embryos (B) display normal D/V axis, but a thinner yolk tube extension (arrowhead) and a protruding telencephalon. At higher magnification, cerebellum (arrowhead in panel D) appears smaller compared to wild-type (arrowhead in panel C). Lateral views, anterior to the left.

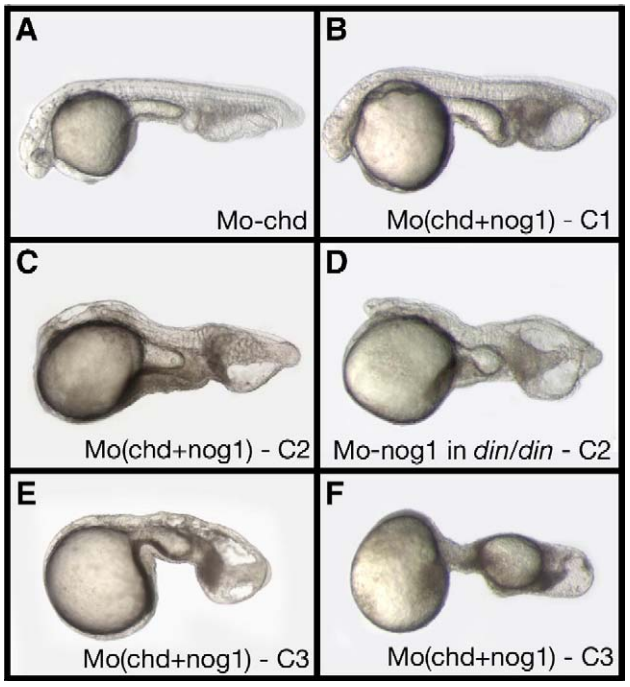

Fig. 3. Inactivation of *noggin1* enhances the ventralization phenotype of *chordin* loss of function. (A) MO-chd-injected embryos at 30 hpf. (B–F) Injection of MO-chd together with MO-nog1 leads to (B) class 1 (C1) embryos corresponding to a weak enhancement of chd phenotype. In class 2 (C2) embryos, the ventralization phenotype following (C) injection of MO-chd and MO-nog1 or (D) injection of MO-nog1 in *chordino* (*din/din*) mutant is more pronounced than in class 1, with loss of most of the head territory. (E, F) In class 3 (C3) embryos, the ventralization after double chd-nog1 MO injection is stronger with an almost complete disappearance of anterior and dorsal territories. Lateral views, anterior to the left.

Results

Within the course of genetic screens (Hammerschmidt et al., 1996; Solnica-Krezel et al., 1996), the *din* and *ogo* mutant embryos were described to share a characteristic ventralized phenotype, with reduction of the head, expansion of the ventral hematopoietic territory and a partial loss of the posterior notochord (Hammerschmidt et al., 1996, Fig. 1A, Miller-Bertoglio et al., 1999, Fig. 1B). However, the phenotype of *chd* loss of function is slightly stronger than loss of function of *sizzled* (compared Figs. 1A to 1B). As described in Yabe et al. (2003), concomitant inactivation of *chd* and *ogo* generate ventralization phenotype similar to *chd* loss of function (Fig. 1C). However, these ventralization phenotypes observed after single or double inactivation of *chd* and/or *ogo* are still less severe than the ventralization phenotypes obtained upon over-expression of *bmp2b* RNA (Figs. 1D–F). Injection of progressive doses of *bmp2b* RNA (from 1 to 20 pg RNA) into 1-cell

Table 1
Noggin1 inactivation enhances ventralization in *chd* morphants or mutants

Morpholino used/ genetic background	Concentration (μM)	*n*	Phenotype (%)			
			wt	C1	C2	C3
MO-chd	100	174	1.2	98.8	0	0
[*din*/+×*din*/+]	–	59	65.7	34.3	0	0
MO-chd/MOa-nog1	100/500	69	–	46.4	49.3	4.3
MO-chd/MOa-nog1	100/750	307	–	34.6	56.6	8.8
MO-chd/MOa-nog1	100/1000	77	–	40.2	41.8	18
MO-chd/MOb-nog1	100/750	66	–	43.9	50	6.1
MO-chd/MOb-nog1	100/1000	86	–	43.5	41.4	15.1
MOa-nog1 in [*din*/+×*din*/+]	750	85	74.7	8.4	16.9	0
MOa-nog1 in [*din*/+×*din*/+]	1000	59	83.0	0	17.0	0

Percentage of embryos (*n*: number of embryos analyzed) of the different phenotypic classes defined in Fig. 3 in function of conditions used (concentration of MO, mutant background).

stage embryos induces much stronger defects, giving rise for the highest dose to complete ventralization and spindle-shaped embryos (Schmid et al., 2000, Fig. 1F). This suggests that, in addition to Chd and Ogo, other Bmp antagonists may be required to pattern the D/V axis.

Gain of function studies we performed in the past suggested that the *noggin1* gene (*nog1*) could be a potential candidate to be involved in the early D/V patterning (Fürthauer et al., 1999). In the zebrafish, we cloned three *noggin* genes and found that their combined expressions recapitulate the different aspects of the expression of the single *noggin* gene of other vertebrates. All three *noggin* when overexpressed are able to dorsalize the embryo. However, only *nog1* is expressed in the fish organizer at blastula and early gastrula stages, in a location and at a time compatible with its potential implication in D/V patterning.

By comparing expression territories of *nog1* with those of *ogo* and *chd*, we found that *ogo* transcripts are located on the ventral side, in a territory similar to *bmp* expression domain (Fig. 1G), compatible with its potential function as a negative feedback regulator of Bmp (Yabe et al., 2003). *Chd* territory of expression is located in a broad dorso-marginal domain that includes the dorsal organizer (Schulte-Merker et al., 1997, Fig. 1H). *Nog1* expression is included within the *chd* expression

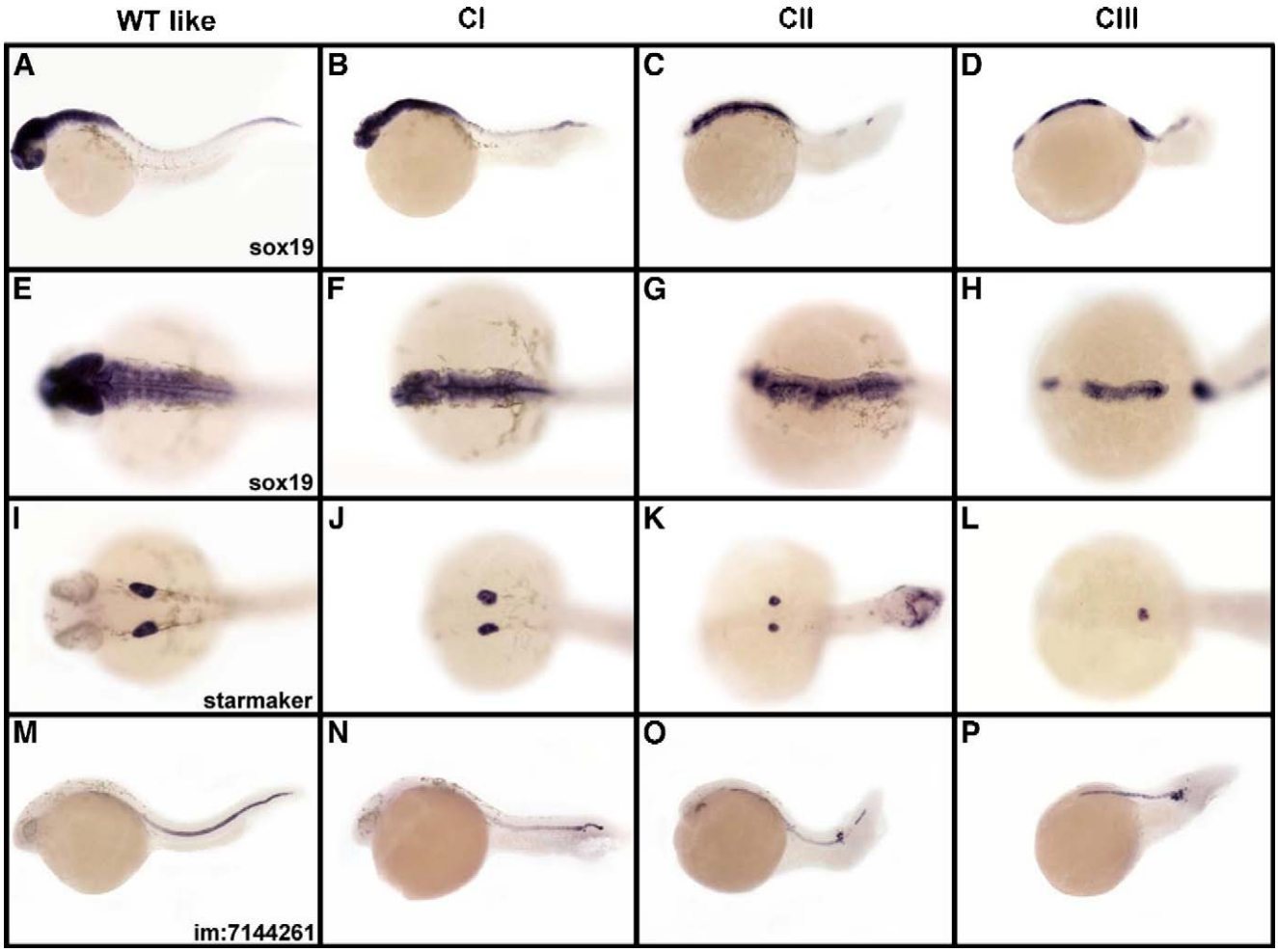

Fig. 4. Analysis of double *chordin–noggin1* morphants for the expression of tissue-specific molecular markers at 30 hpf. Expression at 30 hpf of three different molecular markers, *sox19* labeling the central nervous system, *starmaker* labeling the otic vesicle and *im:7144261* labeling the notochord. (A, E, I, M) Wild-type embryos while the others embryos are injected with MO-chd and MO-nog1 in conditions described in Table 2. (B, F, J, N) Weak aggravation (class I, CI) of the ventralization phenotype, (C, G, K, O) strong ventralization—class II—CII, and (D, H, L, P) extreme ventralization (class 3, CIII). Embryos in lateral view (A–D), (M–P). In dorsal view (E–L), anterior to the left.

domain as it is expressed following the activation of the zygotic genome in a few cells of the dorsal marginal region of the blastoderm (Fürthauer et al., 1999, Fig. 1I). The onset of *nog1* expression was confirmed by RT-PCR. *Nog1* is not expressed maternally, and its zygotic expression starts at the sphere stage (not shown).

Inactivation of noggin1

Both overexpression studies and *nog1* expression pattern suggest that this gene may be involved in the early patterning of the D/V axis. To gain further insights in Nog1 function, we performed knock-down studies by injecting two different morpholinos directed against *nog1* (MOa-nog1 and MOb-nog1) into 1-cell stage embryos (see Materials and methods).

Surprisingly, whatever morpholino used, no D/V patterning defects were ever observed and at 24 hpf the embryos appear strikingly similar to wild-type (compare Figs. 2B to A). The mild morphological abnormalities observed either after injection of MOa-nog1 (500–1000 μM) or MOb-nog1 (750–1500 μM) consisted in a protruding telencephalon, a thinner midbrain–hindbrain boundary and a slender yolk sac extension (Figs. 2B and D, 80%, $n=220$ for 750 μM MOa-nog1) with lower frequency of phenotypes for MOb-nog1 (30%, $n=190$ for 750 μM MOb-nog1). Analysis by whole-mount *in situ* hybridization using a specific marker of telencephalon (*emx1*) either at somitogenesis stages or at 24 hpf failed to reveal any telencephalon abnormalities (not shown). Concomitant injection of MOa-nog1 and MOb-nog1 (800–800 μM) did not enhance the observed phenotype (79%, $n=122$), suggesting that the described defects were already maximum after single injection of MOa-nog1 injection. After 4 days of development, embryos subjected to morpholinos directed against *nog1* lacked all posterior branchial arches, up to the level of the anteriorly located Meckel cartilage, which appeared reduced in size but remained well shaped (not shown).

Double inactivation of chordin and noggin1

Altogether, even though inactivation of *nog1* leads to minor defects at 24 hpf and to rather late branchial arches abnormalities, these results show that *nog1* is not essential by itself for the early establishment of the D/V patterning. However, at gastrula stage, *chd* is expressed in a broad dorsal domain that encompasses the *nog1* expression territory (Figs. 1H, I), suggesting that Chd may compensate for Nog1 loss of function. To test this hypothesis, we performed concomitant inactivation of *nog1* and *chd*. Co-injection of MOa-nog1 (from 500 μM to 1000 μM) together with MO-chd (100 μM) leads to strengthen the ventralization phenotype of *chd* morphant embryos (Fig. 3 and Table 1). Nearly half of the population of injected embryos showed a complete deletion of anterior head and a much more extended hematopoietic territory (Fig. 3C—Table 1) compared to Chd loss of function (Fig. 3A—Table 1). This phenotype was obtained as well when injecting MOa-nog1 (750 or 1000 μM) into a *din/din* background (compare Fig. 3C with D). Furthermore, up to 18% of the embryos belonged to an additional phenotypic class (C3) corresponding to a more dramatic ventralization, with a complete lack of head structures. These embryos were essentially made of ventral tissues such as epidermis and blood (Fig. 3E—Table 1). Among these C3 embryos, a few individuals (3/77 embryos for MO-chd/Moa-nog1 100/1000 μM) displayed an extreme phenotype with constriction of the yolk tube and their blood territory located very posteriorly (Fig. 3F). Comparable classes were obtained using co-injection of MOb-nog1 together with MO-chd (Table 1).

Altogether, these results reveal an amplification of the *chd* phenotype by co-injection of MO-nog1, suggesting a redundant function of Nog1 and Chd on the D/V patterning.

Because a second ventralized mutant *ogo* has been identified in the zebrafish, we tested whether inactivation of *nog1* may also amplify the *ogo* phenotype. Injection of 500 μM MO-ogo resulted in embryos identical to *ogo/ogo* mutants (Fig. 1B, 100% $n=72$). Co-injection of 800 μM MOa-nog1 enhanced this ventralization phenotype as half of the population displayed an enlarged ventral hematopoietic territory similar to *chd* loss of function (58%, $n=156$). On the other hand, the size of the head was not affected and appeared similar to *ogo/ogo* mutant (Fig. 1B).

To better characterize the amplification of the *chd* morphant phenotype by simultaneous loss of function of Nog1, we analyzed the expression of various molecular markers specific of ectodermal or mesodermal tissues at 30 hpf. We first analyzed the expression territory of a pan neural marker *sox19* (Thisse et al., 2001; Agathon et al., 2003). Four classes were defined (ranging from wild-type to class III—CIII) in which the neural

Table 2
Frequency of phenotypic classes in single and double *chd-nog1* morphants at 30 hpf

Morpholinos injected	Concentration (μM)	Marker	*n*	Phenotypes (%)			
				wt like	CI	CII	CIII
MOa-nog1	500	*sox19*	17	100	0	0	0
MOa-nog1	1000	*sox19*	50	100	0	0	0
MO-chd	100	*sox19*	79	36.7	63.3	0	0
MO-chd/ MOa-nog1	100/500	*sox19*	23	34.8	4.4	39.1	21.7
MO-chd/ MOa-nog1	100/1000	*sox19*	191	13.1	12.0	57.6	17.3
MOa-nog1	500	*starmaker*	27	100	0	0	0
MOa-nog1	1000	*starmaker*	20	100	0	0	0
MO-chd	100	*starmaker*	20	75	25	0	0
MO-chd/ MOa-nog1	100/500	*starmaker*	18	16.7	50	33.3	0
MO-chd/ MOa-nog1	100/1000	*starmaker*	30	20	23.3	46.7	10
MOa-nog1	500	*im:7144261*	17	100	0	0	0
MOa-nog1	1000	*im:7144261*	21	100	0	0	0
MO-chd	100	*im:7144261*	139	71.9	28.1	0	0
MO-chd/ MOa-nog1	100/500	*im:7144261*	25	4.0	16.0	20.0	60.0
MO-chd/ MOa-nog1	100/1000	*im:7144261*	22	9.1	9.1	22.7	59.1

Percentage of embryos (n=number of embryos) of the different classes defined in Fig. 4 based on the expression of tissue-specific markers at 30 hpf (*sox19* for central nervous system, *starmaker* for otic vesicle and *im:7144261* for notochord) in function of the concentration (in μM) of the nog1 or chd morpholino-injected.

plate progressively became thinner and shorter (Figs. 4A–H). While CI class is observed for single inactivation of *chd*, the CII and CIII classes were only observed after double inactivation of *chd* and *nog1* (Table 2). In extreme cases (CIII), only discontinuous stretches of neural tube remained (Figs. 4D, H). The second marker used was *starmaker* (Thisse et al., 2001; Söllner et al., 2003) specific of the otic vesicle. Four classes were also defined (Figs. 4I–L), CI showing small otic vesicle (Fig. 4J), CII consisting of smaller, round otic vesicles (Fig. 4K) and CIII showing a unique, small round otic vesicle located at the midline (Fig 4L). For this last class, the otic vesicle appeared located at the anterior extremity of the remaining neural tube. As for the analysis with *sox19*, CII and CIII phenotypes were only found for the double *chd*/*nog1* inactivation (Table 2). We then analyzed the effect of *chd* and *nog1* loss of function on axial mesoderm using a specific notochordal marker *im:7144261* (Thisse and Thisse, 2004). Again, four classes from wild-type to CIII were also defined, CI embryos showing a normal morphology anteriorly but a wavy notochord in the tail region (Fig. 4N). CII embryos were characterized by a shorter axis, with a wild-type notochord interrupted at the level of the anus (Fig. 4O). Finally, CIII embryos displayed a very short notochord, which failed to elongate posterior to the anus (Fig. 4P). As mentioned for sox19 and starmaker, CII and CIII did not exist for single inactivation of *chd* (Table 2).

In summary, this analysis revealed much stronger phenotypes when inhibiting *nog1* and *chd* together than for single inactivation of *chd* or *nog1*.

We then studied the effect of inactivation of *chd* and *nog1* at early developmental stages using various gastrula and early somitogenesis markers specific of ectodermal and mesendodermal territories (Figs. 5, 6 and Table 3). We first analyzed the

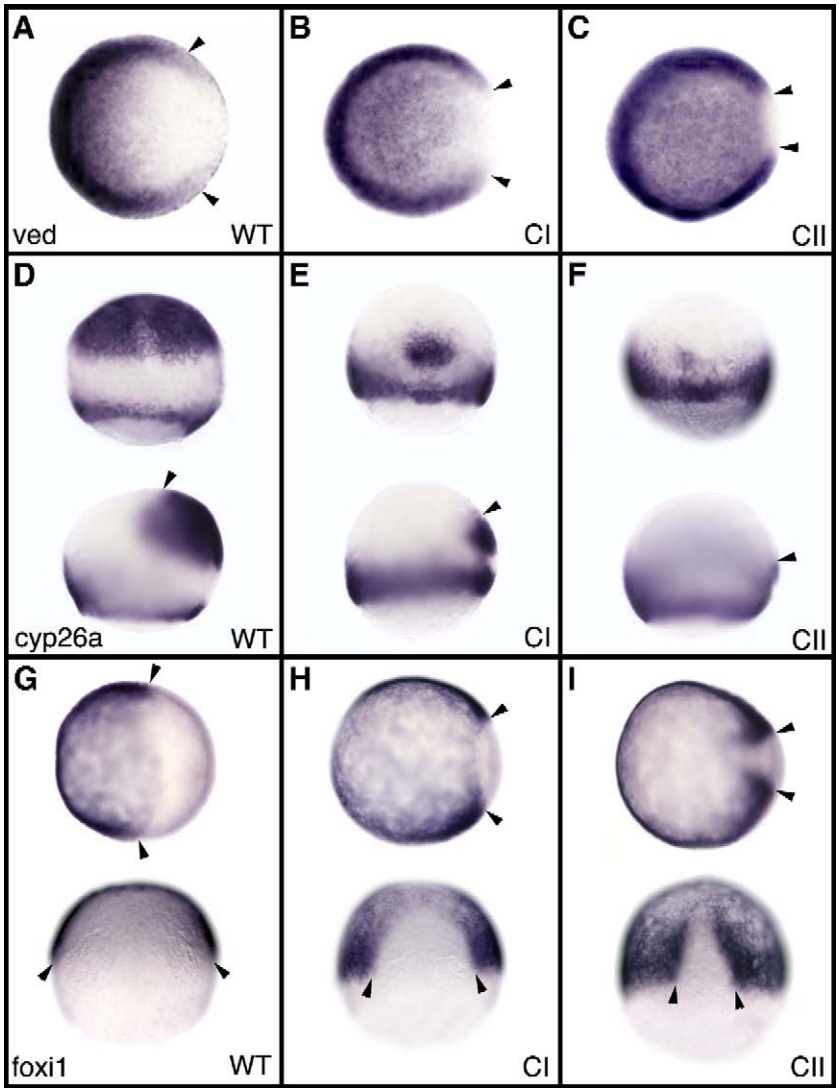

Fig. 5. Analysis of double *chordin–noggin1* morphants for the expression of early molecular markers. Expression of *ved* (A–C), a Bmp target gene expressed in the ventral part of the gastrula, *cyp26a* (D–F) expressed at the margin and in anterior neural plate, *foxi1* (G–I), a marker of presumptive epidermis at gastrula stage. (A, D, G) Wild type (WT), (B, E, H) injection of 100 μM of MO-chd (class I, CI), (C, F, I) injection of 100–800 μM chd-nog1 MOs (class II, CII). Arrowheads in panels A–C indicate the dorsal limits of *ved* expression. Arrowheads in panels D–F indicate the anterior limit of the neural plate labeled with *cyp26a* and arrowheads in G–I, the dorsal limits of the presumptive epidermis labeled with *foxi1*. Embryos are in animal pole view dorsal to the right in panels A–C and G–I upper panels. Dorsal views animal pole up in panels D–E and G–I lower panels.

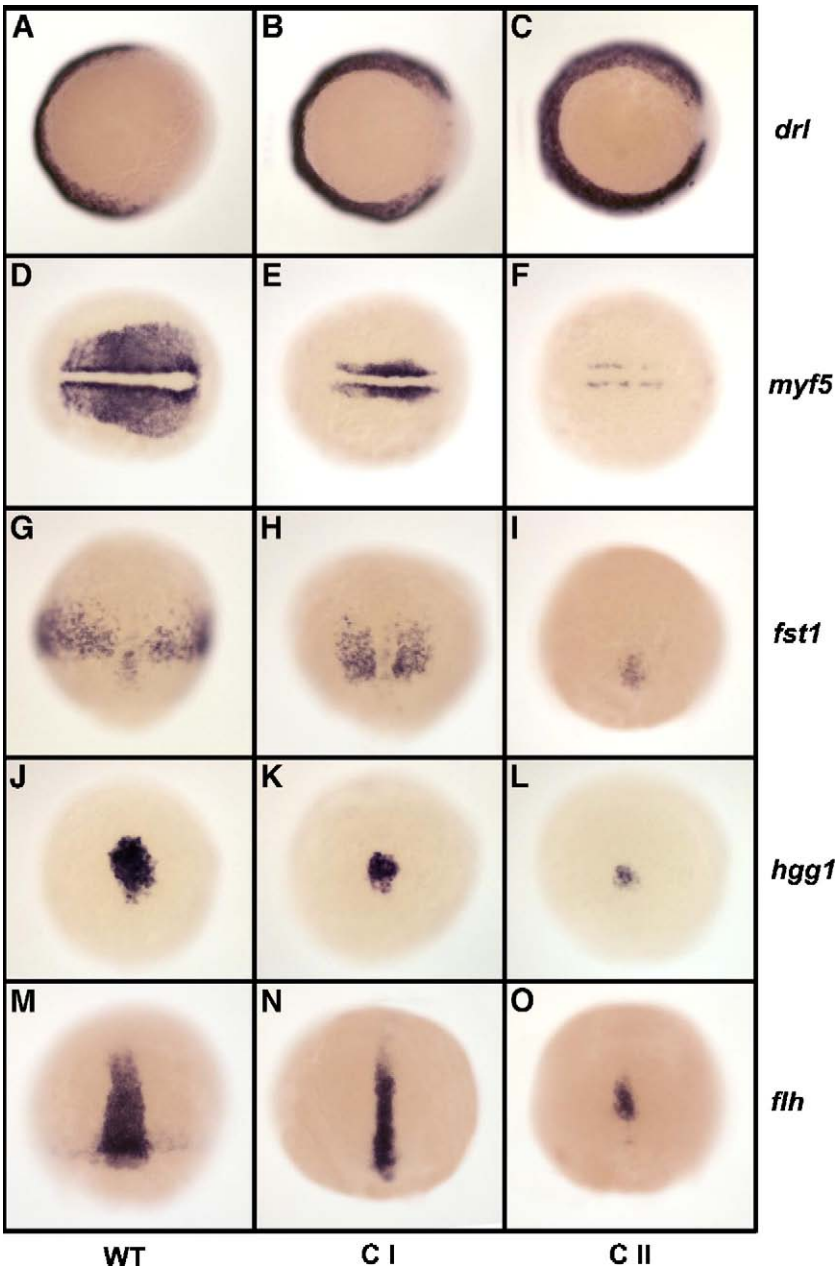

Fig. 6. Analysis of double *chordin–noggin1* morphants with endomesodermal markers. (A–C) Expression of *draculin* (*drl*) specific of presumptive hematopoietic territory at 70% epiboly. (D–F) Expression of the paraxial marker *myf5* at the 3-somite stage. (G–I) Expression of the cephalic mesendodermal marker *follistatin1* (*fst1*) at 80% epiboly. (J–L) Expression of the prechordal plate marker *hgg1* which labels the presumptive hatching gland at 75% epiboly. (M–O) Expression of the notochordal marker *floating-head* (*flh*) at 75% epiboly. (A, D, G, J, M) Wild-type embryos (B, E, H, K, N), 100 μM MO-chd-injected embryos (C, F, I, L, O) 100–800 μM chd-nog1 MOs-injected embryos. (A–C) Vegetal pole views, dorsal to the right. (D–F) Dorsal views anterior to the left. (G–O) Dorsal views, animal pole up.

expression of *ved*, a target gene of the Bmp signaling pathway (Gilardelli et al., 2004). In wild-type, expression of *ved* is detected in the ventral part of the gastrula and is excluded from the dorsal side of the embryo at 50% epiboly (Thisse et al., 2001, Fig. 5A). In embryos injected with 100 μM of MO-chd, expression of *ved* was expanded towards dorsal (Fig. 5B). In embryos injected with both morpholinos against *chd* and *nog1* (100 μM, 800 μM), this enlargement was even more pronounced, showing a strong ventral expansion of *ved* (Fig. 5C). Under the same experimental conditions, the anterior neurectodermal territory labeled with *cyp26a* (Thisse et al., 2001; Fürthauer et al., 2004) appeared strongly reduced in embryos injected with MO-chd (Fig. 5E) and disappeared almost completely in double morphants (Fig. 5F). On the other hand, *foxi1*, specific of presumptive epidermis (Thisse et al., 2001; Fürthauer et al., 2004), was expanded on the dorsal side of the embryo, with a much stronger expansion in the case of double inactivation of *chd* and *nog1* (Figs. 5G–I).

During gastrulation, expression of *draculin* (*drl*), a marker specific of presumptive ventral hematopoietic mesoderm (Herbomel et al., 1999; Thisse et al., 2001), extended toward

Table 3
Frequency of phenotypic classes obtained for single and double *chd-nog1* morphants at early developmental stages

Morpholinos injected	Concentration (μM)	Probe	*n*	Phenotype (%)		
				wt	CI	CII
MOa-nog1	800	*ved*	68	100	0	0
MO-chd	100	*ved*	48	25	50	25
MO-chd/MOa-nog1	100/800	*ved*	76	14.5	42.1	43.4
MOa-nog1	800	*cyp26a*	19	100	0	0
MO-chd	100	*cyp26a*	35	17.1	82.9	0
MO-chd/MOa-nog1	100/800	*cyp26a*	31	25.8	54.8	19.4
MOa-nog1	800	*foxi1*	36	100	0	0
MO-chd	100	*foxi1*	37	5.4	94.6	0
MO-chd/MOa-nog1	100/800	*foxi1*	40	25.0	47.5	27.5
MOa-nog1	800	*drl*	32	100	0	0
MO-chd	100	*drl*	60	0	85	15
MO-chd/MOa-nog1	100/800	*drl*	77	7.8	27.3	64.9
MOa-nog1	800	*myf5*	58	100	0	0
MO-chd	100	*myf5*	62	8.1	88.7	3.2
MO-chd/MOa-nog1	100/800	*myf5*	59	6.8	52.5	40.7
MOa-nog1	800	*fst1*	49	100	0	0
MO-chd	100	*fst1*	51	7.8	47.1	45.1
MO-chd/MOa-nog1	100/800	*fst1*	30	3.3	26.7	70
MOa-nog1	800	*hgg1*	50	60	32	8
MO-chd	100	*hgg1*	48	25	66.7	8.3
MO-chd/MOa-nog1	100/800	*hgg1*	57	28.1	45.6	26.3
MOa-nog1	800	*flh*	84	100	0	0
MO-chd	100	*flh*	116	11.5	70.1	18.4
MO-chd/MOa-nog1	100/800	*flh*	199	7.5	40.8	51.7

Percentage of embryos (*n* = number of embryos) of the different classes defined in Figs. 5 and 6 on the expression of tissue-specific markers at early developmental stages (*ved* for the ventral part of the gastrula, *cyp26a* for the margin and the anterior part of neural plate, *foxi1* for the presumptive epidermis, *drl* for the hematopoietic mesoderm, *myf5* for the paraxial mesoderm, *fst1* for the cephalic mesendoderm, *hgg1* for the prechordal plate and *flh* for the notochord) in function of the concentration (in μM) of MOa-nog1 and/or MO-chd-injected.

dorsal in embryos injected with MO-chd (Fig. 6B and Table 3). This enlargement of ventral mesoderm was even more pronounced in *chd/nog1* morphants (Fig. 6C). At early somitogenesis stages, *myf5*, a muscle-specific marker labeling the segmental plate (Thisse et al., 2001) appeared strongly reduced after injection of MO-chd (Fig. 6E) remaining only detectable in adaxial cells and in adjacent paraxial mesoderm. In embryos injected with MO-chd and MOa-nog1, *myf5* labeling was almost absent and remained only in a few adaxial cells (Fig. 6F). Similarly, cephalic mesendoderm, observed using *follistatin1* (*fst1*—Bauer et al., 1998; Thisse et al., 2001), was reduced along the D/V axis and almost absent after double inactivation of *chd* and *nog1* (Figs. 6G–I). In the axis, at gastrulation, analysis of *hgg1* (Thisse et al., 1994) revealed that the prechordal plate was reduced after inactivation of *chd* and almost absent in double morphants (Figs. 6J–L). Finally, expression of *floating head* (*flh*—Talbot et al., 1995) specific of chorda mesoderm appeared thinner in *chd* morphant and was further reduced along the antero-posterior axis in embryos injected with both MO-chd and MOa-nog1 (Figs. 6M–O).

Altogether, this analysis using specific molecular markers shows that, already at early developmental stages, the double inactivation of *chd* and *nog1* strongly enhances the ventralization phenotype observed after Chd loss of function.

Rescue of chd-nog1 morphants phenotype by addition of fgf8 or follistatin1 RNA

Because Chd and Nog1 negatively interact with Bmps by direct binding, the aggravation of the ventralization phenotype resulting from the inactivation of *nog1* in *chd* loss of function context strongly suggests that Nog1 is responsible for the Bmp antagonistic activity remaining in the *chd* mutant. To demonstrate that the effect of Nog1 is due to its Bmp inhibitory properties, we investigated whether we could rescue the ventralization phenotypes obtained for *chd-nog1* morphants by other factors inhibiting Bmp activity. To perform such rescue experiments, we chose *fgf8*, which controls the expression of the *bmp* genes via the stimulation of the FGF receptor 1 and the activation of the Ras/MAP kinase signaling pathway (Fürthauer et al., 2004). In addition, we used another factor, *follistatin1* (*fst1*), known to be able to antagonize Bmp activity and for which its misexpression leads to dorsalization phenotypes (Hemmati-Brivanlou et al., 1994; Bauer et al., 1998, our own results).

All embryos injected with MO-chd or MO-chd plus MOa-nog1 showed ventralization (Fig. 7). On the other hand, co-injections of high dose of *fgf8* or *fst1* RNA (15 pg and 400 pg respectively) in *chd* or *chd-nog1* morphants reverted this phenotype to dorsalization, identical to the dorsalization phenotype observed after single injection of *fgf8* or *fst1* RNA (not shown). After co-injection of lower doses of *fgf8* or *fst1* RNA (5 pg and 50 pg respectively), a small proportion of embryos (between 3% *n* = 62 and 31% *n* = 93) were ventralized while the others presented a wild-type-like or a dorsalized morphology (Fig. 7).

In this set of experiments, the percentage of dorsalized embryos was much higher for the rescue of chd (73% *n* = 62 for fgf8 and 57% *n* = 86 for fst1) than for the rescue of chd-nog1 morphants (49% *n* = 87 for fgf8 and 30% *n* = 93 for fst1). Due to the additional lack of nog1, injection of the same amounts of FGF8 or Fst1 led to a weaker dorsalization in *chd-nog1* morphants than in *chd* morphants.

Additional analysis performed by *in situ* hybridization looking at the expression of *foxi1*, *ved* and *cyp26a* confirmed that the rescue of *chd-nog1* morphants phenotype by addition of *fgf8* or *fst1* RNA is already effective at gastrula stage (not shown).

Follistatin-like 2 (Fstl2): another player involved in the control of Bmp activity

Our previous experiments demonstrate that Nog1 carries an anti-*bmp* activity still present in the *chd* mutant and explains, at least in part, the remaining dorsal tissues observed in *din/din* mutant. Nevertheless, after double inactivation of *chd* and *nog1*, the ventralization phenotype is less severe than the one observed after injection of high dose of *bmp* RNA (Fig. 1F). This suggests that other factors sharing an anti-Bmp activity may be present in the early embryo to establish the D/V axis.

In *Xenopus*, Follistatin has been suggested to play such a role, but in zebrafish, *follistatin1* (*fst1*) transcripts are first detected at 70% epiboly in cephalic mesendoderm (Bauer et al., 1998;

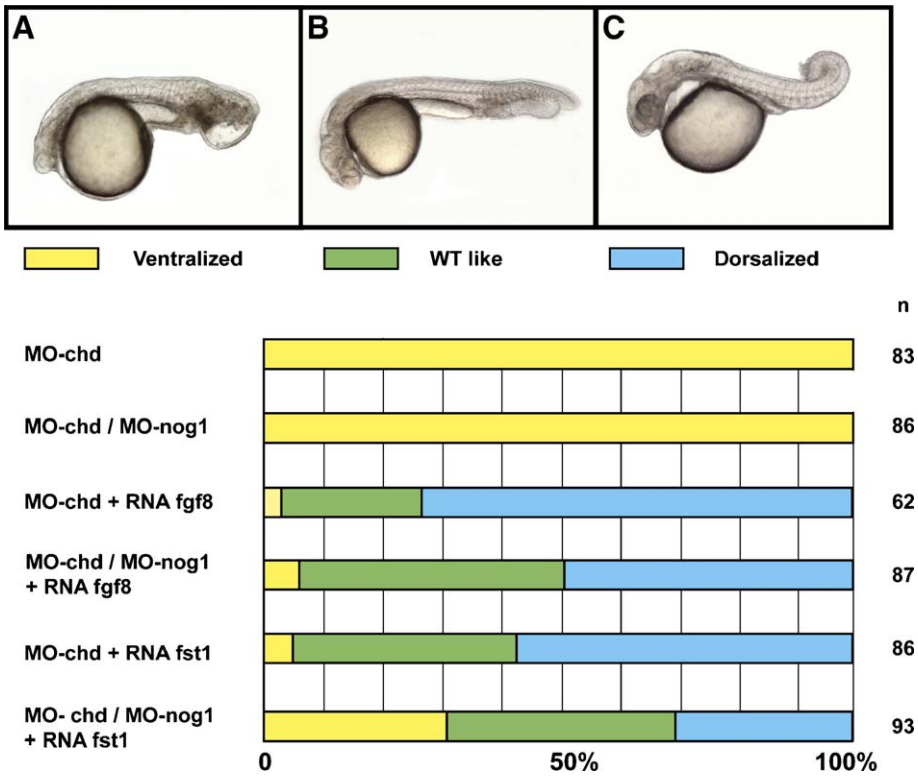

Fig. 7. Fgf8 and Fst1 overexpression rescues *chordin* and *chordin–noggin1* morphants. (A) Example of a ventralization phenotype observed after injection of *chd* or *chd-nog1* morpholinos. (B) Example of wild-type like morphology obtained after injection of *fgf8* or *fst1* RNA into *chd* or *chd-nog1* morphants (C). Example of a dorsalization phenotype observed after injection of *fgf8* or *fst1* RNA into *chd* or *chd-nog1* morphants. Embryos are observed at 30 hpf in lateral view, anterior to the left. Lower panel: the horizontal bars represent the percentage of embryos displaying a ventralized phenotype (yellow), a wild-type like morphology (green) or a dorsalized phenotype (blue) in *chd* morphants (MO-chd, 100 μM), double *chd-nog1* morphants (MO-chd/MO-nog1—100 μM/800 μM), in *chd* or *chd-nog1* morphants injected with 5 pg of *fgf8* RNA (MO-chd+RNA *fgf8*; MO-chd/MO-nog1+RNA *fgf8*, respectively) or with 50 pg of *fst1* RNA (MO-chd+RNA fst1; MO-chd/MO-nog1+RNA fst1, respectively). Due to the lack of two Bmp inhibitors, the rescue of ventralization phenotype (wild-type-like and dorsalized phenotypes) by *fgf8* and *fst1* is less efficient in double *chd-nog1* morphants than in single *chd* morphants. *n*: number of embryos analyzed.

Thisse et al., 2001), too late for assuming that Fst1 controls the D/V axis formation. In agreement with this hypothesis, inactivation of *fst1* by morpholino injection results in a late phenotype characterized by the lack of posterior branchial arches while the D/V patterning remains unaffected (not shown). In addition, injection of MO-fst1 failed to amplify the ventralization phenotype of *chd* morphant (not shown).

In a search for potential candidates that may control the establishment of the D/V axis, we identified a second *follistatin* gene, *follistatin2* (*fst2*, Fig. S1). As for *fst1*, overexpression of *fst2* by sense RNA injection causes dorsalization (not shown). Analysis of *fst2* expression shows that it begins at the 14-somite stage in the proximal region of ventral and dorsal parts of the somites. This myotomal expression is maintained until the end of tail elongation. Later on, *fst2* transcripts are detected in anterior branchial arches (Fig. S2).

Therefore, while these proteins carry an anti-Bmp activity (Bauer et al., 1998; our unpublished observations), the expression pattern of the two zebrafish *follistatin* genes *fst1* (Bauer et al., 1998; Thisse et al., 2001) and *fst2* (Fig. S2) is not supportive of their implication during early axis formation.

However, a growing number of proteins have been described to share sequence similarities to Follistatin, defining thereby the Follistatin-domain family (Phillips and de Kretser, 1998). The

Fig. 8. Follistatin-like 2 (Fstl2) is involved in the control of the D/V axis formation. (A) Expression of *fstl2* starts at the onset of gastrulation in the deep cells of the embryonic shield (sh). (B) At 60% epiboly, *fstl2* transcripts are observed in notochord (n) as well as in the yolk syncytial layer (ysl). (C–D) At 75% epiboly, expression is restricted to the notochord. (E) Morphological analysis of morphant phenotypes at 30 hpf. Single *fstl2* or *nog1* morphants as well as double *fstl2–nog1* morphants display D/V axis similar to wild-type (WT like). *Chd* morphants or mutants display a ventralization phenotype characterized by a small head and an enlarged hematopoietic territory (C1). Double *chd-fstl2*; *chd-nog1* or triple *chd-fstl2-nog1* morphants display stronger ventralization phenotype with very small head and strong enlargement of ventro-posterior territories (C2) or an extreme ventralization phenotype with lack of head (C3). Graphs underneath each picture represent the percentage of embryos observed for the corresponding class observed for the different combination of morpholino injected described in the table in panel H. (F) Analysis of single, double and triple morphants with *ved*, a marker of ventral territories at gastrula stage. Embryos are in vegetal pole view, dorsal to the right. Whereas at 50% epiboly, in wild-type, *ved* is detected in the ventral part of the gastrula, in CI, expression of *ved* is expanded towards dorsal. In CII, this enlargement is even more pronounced. (G) Analysis by *in situ* hybridization of single, double and triple morphants using *cyp26a*, a marker of margin and of anterior neural plate at gastrula stage. Embryos are in lateral view, animal pole up. Compared to wild-type-like embryos, in CI, the anterior neurectodermal territory labeled with *cyp26a* appears strongly reduced while it is almost absent in CII. (I) For the different combinations of morpholinos used, the table records the number and the percentage of embryos for the classes described in panels F and G and analyzed by *in situ* hybridization with *ved* and *cyp26a*.

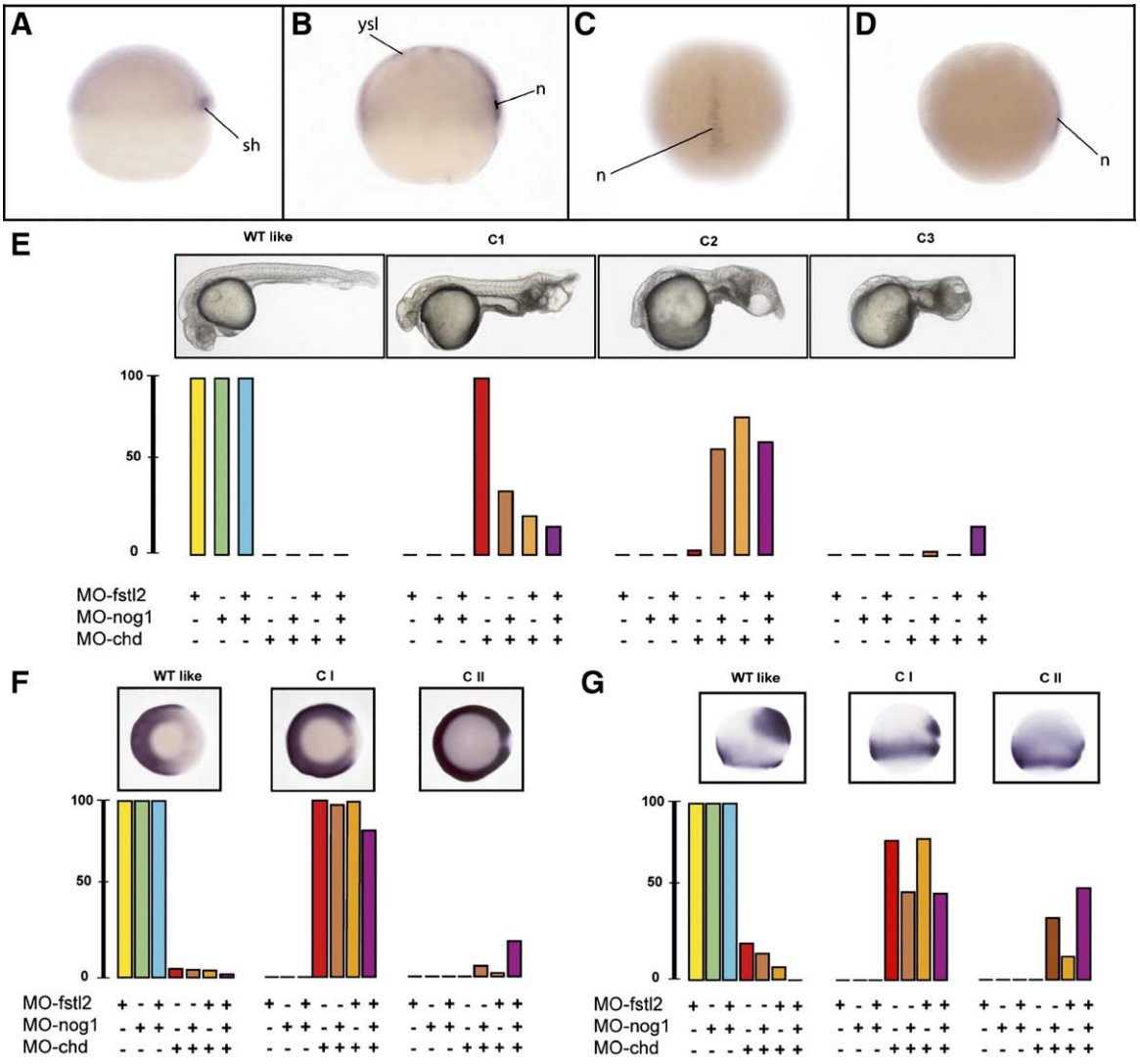

H

Morpholino injected	Concentration (μM)	n	Phenotype (%) wt	C1	C2	C3
MO-fstl2	1000	131	100	0	0	0
MOa-nog1	500	200	100	0	0	0
MO-fstl2 / MOa-nog1	1000/500	236	100	0	0	0
MO-chd	100	288	0	98	2	0
MO-chd / MOa-nog1	100/500	392	0	27	71	2
MO-chd / MO-fstl2	100/1000	321	0	18	82	0
MO-chd / MOa-nog1/MO-fstl2	100/500/1000	337	0	14	74	12

I

Morpholinos injected	Concentration(μM)	Probe	n	Phenotype (%) wt	CI	CII
MO-fstl2	1000	ved	100	100	0	0
MOa-nog1	500	ved	118	100	0	0
MO-fstl2 / MOa-nog1	1000/500	ved	126	100	0	0
MO-chd	100	ved	149	5	95	0
MO-chd / MOa-nog1	100/500	ved	165	5	89	6
MO-chd / MO-fstl2	100/1000	ved	166	4	94	2
MO-chd / MOa-nog1/MO-fstl2	100/500/1000	ved	134	2	79	19
MO-fstl2	1000	cyp26a	51	100	0	0
MOa-nog1	500	cyp26a	67	100	0	0
MO-fstl2 / MOa-nog1	1000/500	cyp26a	46	100	0	0
MO-chd	100	cyp26a	43	21	79	0
MO-chd / MOa-nog1	100/500	cyp26a	40	15	50	35
MO-chd / MO-fstl2	100/1000	cyp26a	59	7	80	13
MO-chd / MOa-nog1/MO-fstl2	100/500/1000	cyp26a	53	0	49	51

common feature of these proteins is the occurrence of a domain of nearly 70 amino acids containing 10 cysteine residues at strongly conserved positions (Patthy and Nikolics, 1993). All Follistatin family proteins appear to be secreted, being either released in the extracellular space or acting as transmembrane proteins. Based on the activin-binding activity of Follistatin, follistatin modules have been proposed to mediate growth factors binding (Patthy and Nikolics, 1993). In addition, several studies suggest that at least one other Follistatin-module containing factor, namely Follistatin-like protein (Fstl, also named Follistatin-related protein, Frp) is implicated in the regulation of TGFβ signaling. *Fstl* was originally isolated as a TGFβ1 inducible gene, in accordance with its potential feedback inhibitor function (Shibanuma et al., 1993). *Fstl* is expressed in the organizing center and chordamesoderm of the mouse, chick and *Xenopus* embryos, suggesting its implication in the early axis formation of several vertebrate species (Patel et al., 1996; Okabayashi et al., 1999; De Groot et al., 2000). While overexpression of *fstl* in *Xenopus* embryos appears to have no effect on development (Okabayashi et al., 1999), the inhibition of *fstl* function through antisense oligonucleotides in the chick results in axial defects (Towers et al., 1999).

In zebrafish, we isolated two *follistatin-like* (*fstl*) genes, *fstl1* and *fstl2*, which can be aligned along their whole peptide sequence with their *Xenopus*, chicken and mouse counterparts (Fig. S3). Phylogenetic analysis confirmed that both fish genes belong to the Fstl branch of the Follistatin-domain family (Fig. S3B).

Fstl2 becomes first detectable at the onset of gastrulation (Fig. 8A and Fig. S4). Transcripts localize to the deep layer of the embryonic shield, a territory also expressing *nog1*. Weak *fstl2* expression is also detected in the extraembryonic yolk syncytial layer (Fig. 8B). The expression of *fstl2* in the axial mesendoderm is maintained throughout gastrulation (Figs. 8C, D). In contrast, expression of *fstl1* is not detectable at gastrula stage and first transcripts appear at early somitogenesis in adaxial cells (Fig. S5). Therefore, the expression of *fstl2* at early developmental stages suggests a possible involvement of this gene in axis formation while *fstl1* is expressed too late to favor a possible function of this gene in this process.

In agreement with previous report in *Xenopus* (Okabayashi et al., 1999), we found that overexpression of Fstl2 by injection of sense RNA (from 10 pg up to 600 pg, $n > 100$ for each condition) at the 1-cell stage failed to affect the embryonic development. As well, inactivation of *fstl2* through antisense morpholino injection did not affect the D/V patterning. Embryos were analyzed based on their morphology at 30 hpf or for the expression of specific molecular markers at gastrula stage, *cyp26a* for the dorsal neurectoderm as well as *ved* for the ventral territories. For all concentrations used (up to 1000 μM), injected embryos appeared normal for the formation of the D/V axis and 100% embryos displayed wild-type like morphology and wild-type expression of the molecular markers used. Double inactivation of *nog1* (MOa-nog1 500 μM) and *fstl2* (MO-fstl2 1000 μM) also failed to affect this process. Nevertheless, similarly to the enhancement of *chd* phenotype by additional inactivation of *nog1*, inactivation of *fstl2* strongly enhanced the ventralization phenotypes observed in *chd* morphants. Finally, the triple inactivation of Chd, Nog1 and Fstl2 did not result in new phenotypes. Nevertheless, the percentage of strongly ventralized embryos was increased, reflecting a much higher penetrance of this phenotype (Fig. 8). Altogether, our data demonstrate that, in addition to Chd, two other factors, Nog1 and Fstl2, are required at blastula and early gastrula stages to inhibit Bmp activity on the dorsal side of the zebrafish embryo.

Discussion

The genetic dissection of the D/V patterning of the zebrafish embryo identified several dorsalized mutations (Mullins et al., 1996) including mutations affecting the morphogenes of the D/V axis, namely *bmp2b* (*swirl*) (Kishimoto et al., 1997) and *bmp7* (*snailhouse*) (Dick et al., 2000; Schmid et al., 2000) as well as two ventralized mutants called *dino* (Hammerschmidt et al., 1996) and *ogon* corresponding respectively to inactivation of *chordin* or *sizzled* (Schulte-Merker et al., 1997; Yabe et al., 2003; Martyn and Schulte-Merker, 2003). Loss of function of these two Bmp antagonists results in expanding the ventral territories (epidermis and ventral hematopoietic mesoderm) associated with corresponding reduction of the dorsal ones, brain and dorsal mesoderm. Nevertheless, embryos lacking either the *chd* or *ogo* genes or both still display substantial amount of dorsal and dorso-lateral structures (neural tube, paraxial mesoderm) compared to completely ventralized embryos resulting from overexpression of Bmp (Figs. 1E, F). This strongly suggests that other Bmp antagonists may be responsible for the formation of the dorsal tissues remaining in *chd*/*ogo* double mutants.

Various candidates for carrying such a function have been reported in other species. In particular, Noggin (Zimmerman et al., 1996) and Follistatin (Fainsod et al., 1997) were shown to be able to antagonize Bmp activity *in vivo*. In zebrafish as well, overexpression of Noggin or Follistatin results in strong dorsalization phenotypes (Bauer et al., 1998; Fürthauer et al., 1999).

Likely due to the teleosts whole genome duplication, several *noggin* and *follistatin* genes are present in the zebrafish. Three *noggin* genes were identified (Fürthauer et al., 1999) but only one, *nog1*, is expressed early enough and at the right place to play a role in the establishment of the D/V patterning. However, we show here that its single inactivation, while strongly affecting formation of the branchial arches at late stages, has no effect on early embryonic development. Because *nog1* expression is included within the *chd* expression domain, we studied the effect of the double inactivation of *chd* plus *nog1*. Inactivation by morpholino knock-down of *nog1* in either *chd* morphants or in homozygous *din/din* mutants strongly amplifies the *chd* ventralization phenotype. This clearly demonstrates that *nog1* acts redundantly to *chd* and is responsible, at least in part for the remaining dorsal and dorso-lateral tissues observed in *chd* mutants. As well, *nog1* loss of function is able to amplify the ventralization phenotype of the second ventralized mutant, *ogo*. The gene inactivated in this mutant *sizzled* has recently been shown to bind and inhibit Tolloid (Lee et al., 2006; Muraoka et al., 2006). Therefore, inactivation of *sizzled* in an *ogo* mutant

results in an upregulation of Tolloid and in a downregulation of Chordin. In consequence, the *ogo* mutant phenotype can be considered as a weak mutant of *chordin*, which can be enhanced by simultaneous loss of *nog1*.

We further analyzed the implication of other factors in the D/V patterning, namely the *follistatin* genes. To do so, we cloned two *follistatin* genes and found that *fst2* is expressed during late development in a subset of branchial arches. Because of its late expression, this gene is likely not to be involved in early patterning, even though when overexpressed, this results in a dorsalization phenotype showing its ability to antagonize the Bmp activity. Similarly, *fst1*, which starts to be expressed by 70% epiboly in cephalic mesendoderm, is able to antagonize Bmp activity in gain of function experiments. However, *fst1* is expressed too late to play a major role in D/V axis formation. Indeed, inactivation of *fst1* results solely in deletion of posterior branchial arches and failed to amplify the ventralization phenotype of *chd* morphants.

In *Xenopus*, recent studies revealed that the depletion of *chd*, *nog* and *fst* results in a catastrophic loss of dorsal development, with excessive amounts of ventral tissues at the expense of dorsal structures (Khokha et al., 2005). Inactivation of two of these Bmp antagonists has only a weak effect. Similarly in the mouse, double inactivation of *chd* and *nog* affects only the development of prosencephalon (Bachiller et al., 2000). In contrast, we show here, in the zebrafish, that double inactivation of *chd* and *nog1* results in embryos displaying a much stronger ventralization phenotype. Nevertheless, the triple inactivation of *chd*, *nog* and *fst* in *Xenopus* has a more dramatic effect than double *chd*, *nog* inactivation in the fish, suggesting that other Bmp antagonists may exist. We show here that Follistatin itself does not carry this function.

In a search for other potential candidates to carry this function, we identified two *follistatin-like* genes. While *fstl1* is expressed too late to assume such a role, *fstl2* is expressed early on and in the fish organizer. As described in *Xenopus*, we found that overexpression of *follistatin-like* factors has no effect on zebrafish development. Nevertheless, inactivation of *fstl2* by morpholino knock-down strongly enhances the *chd* ventralization phenotype in a way similar to what we observed for *nog1*. In addition, triple inactivation of *chd*, *nog1* and *fstl2* increases the frequency of strong ventralized phenotype. Therefore, it appears that the function performed by Fst in *Xenopus* is likely to be carried by Fstl2 in zebrafish. However, while Fstl2 is involved in establishment of D/V patterning, it likely requires a still unknown cofactor to bind and inhibit BMP activity.

In conclusion, we show here that Chd appears to be the main Bmp antagonist sufficient to maintain a proper gradient of Bmp activity. In zebrafish, most of the remaining dorsal and dorsolateral territories, in both the mesodermal and ectodermal layers, still present in *chd* mutants result from the anti-Bmp activity carried by Nog1 and Fstl2 at blastula and gastrula stages.

Acknowledgments

We thank Marie Thisse for her pictures of embryos overexpressing Bmp. We thank Sandrine Geschier for taking care of the fish. This work was supported by funds from the Centre National de la Recherche Scientifique, the Institut National de la Santé et de la Recherche Médicale, the Association pour la Recherche contre le Cancer, the Ligue de Recherche contre le Cancer, the Cancéropole, the ACI Biologie du Développement et Physiologie Intégrative No. 311 and the National Institute of Health (R01 RR15402-04).

Appendix A. Supplementary data

Supplementary data associated with this article can be found, in the online version, at doi:10.1016/j.ydbio.2006.07.002.

References

Agathon, A., et al., 2003. The molecular nature of the zebrafish tail organizer. Nature 424, 448–452.

Bachiller, D., et al., 2000. The organizer factors Chordin and Noggin are required for mouse forebrain development. Nature 403, 658–661.

Bauer, H., et al., 1998. Follistatin and noggin are excluded from the zebrafish organizer. Dev. Biol. 204, 488–507.

Connors, S.A., et al., 1999. The role of tolloid/mini fin in dorsoventral pattern formation of the zebrafish embryo. Development 126, 3119–3130.

De Groot, E., et al., 2000. Expression patterns of follistatin and two follistatin-related proteins during mouse development. Int. J. Dev. Biol. 44, 327–330.

Dick, A., et al., 2000. Essential role of Bmp7 snailhouse and its prodomain in dorsoventral patterning of the zebrafish embryo. Development 127, 343–354.

Fainsod, A., et al., 1997. The dorsalizing and neural inducing gene follistatin is an antagonist of BMP-4. Mech. Dev. 63, 39–50.

Fürthauer, M., et al., 1999. Three different noggin genes antagonize the activity of bone morphogenetic proteins in the zebrafish embryo. Dev. Biol. 214, 181–196.

Fürthauer, M., et al., 2004. Fgf signalling controls the dorsoventral patterning of the zebrafish embryo. Development 131, 2853–2864.

Gilardelli, C.N., et al., 2004. Functional and hierarchical interactions among zebrafish vox/vent homeobox genes. Dev. Dyn. 230, 494–508.

Hammerschmidt, M., et al., 1996. *dino* and *mercedes*, two genes regulating dorsal development in the zebrafish embryo. Development 123, 95–102.

Hemmati-Brivanlou, A., et al., 1994. Follistatin, an antagonist of activin, is expressed in the Spemann organizer and displays direct neuralizing activity. Cell 77, 283–295.

Herbomel, P., et al., 1999. Ontogeny and behaviour of early macrophages in the zebrafish embryo. Development 126, 3735–3745.

Khokha, M.K., et al., 2005. Depletion of three BMP antagonists from Spemann's organizer leads to a catastrophic loss of dorsal structures. Dev. Cell 8, 401–411.

Kishimoto, Y., et al., 1997. The molecular nature of zebrafish swirl: BMP2 function is essential during early dorsoventral patterning. Development 124, 4457–4466.

Lee, H.X., et al., 2006. Embryonic dorsal–ventral signaling: secreted frizzled-related proteins as inhibitors of tolloid proteinases. Cell 124, 147–159.

Marques, G., et al., 1997. Production of a DPP activity gradient in the early *Drosophila* embryo through the opposing actions of the SOG and TLD proteins. Cell 91, 417–426.

Martyn, U., Schulte-Merker, S., 2003. The ventralized ogon mutant phenotype is caused by a mutation in the zebrafish homologue of Sizzled, a secreted Frizzled-related protein. Dev. Biol. 260, 58–67.

Miller-Bertoglio, V.E., et al., 1997. Differential regulation of chordin expression domains in mutant zebrafish. Dev. Biol. 192, 537–550.

Miller-Bertoglio, V., et al., 1999. Maternal and zygotic activity of the zebrafish ogon locus antagonizes BMP signaling. Dev. Biol. 214, 72–86.

Mullins, M.C., et al., 1996. Genes establishing dorsoventral pattern formation in the zebrafish embryo: the ventral specifying genes. Development 123, 81–93.

Muraoka, O., et al., 2006. Sizzled controls dorso-ventral polarity by repressing cleavage of the Chordin protein. Nat. Cell Biol. 4, 329–338.

Nguyen, V.H., et al., 1998. Ventral and lateral regions of the zebrafish gastrula, including the neural crest progenitors, are established by a bmp2b/swirl pathway of genes. Dev. Biol. 199, 93–110.

Okabayashi, K., et al., 1999. cDNA cloning and distribution of the *Xenopus* follistatin-related protein. Biochem. Biophys. Res. Commun. 254, 42–48.

Patel, K., et al., 1996. Cloning and early dorsal axial expression of Flik, a chick follistatin-related gene: evidence for involvement in dorsalization/neural induction. Dev. Biol. 178, 327–342.

Patthy, L., Nikolics, K., 1993. Functions of agrin and agrin-related proteins. Trends Neurosci. 16, 76–81.

Phillips, D.J., de Kretser, D.M., 1998. Follistatin: a multifunctional regulatory protein. Front. Neuroendocrinol. 19, 287–322.

Piccolo, S., et al., 1996. Dorsoventral patterning in *Xenopus*: inhibition of ventral signals by direct binding of chordin to BMP-4. Cell 86, 589–598.

Piccolo, S., et al., 1997. Cleavage of Chordin by Xolloid metalloprotease suggests a role for proteolytic processing in the regulation of Spemann organizer activity. Cell 913, 407–416.

Schmid, B., et al., 2000. Equivalent genetic roles for bmp7/snailhouse and bmp2b/swirl in dorsoventral pattern formation. Development 127, 957–967.

Schulte-Merker, S., et al., 1997. The zebrafish organizer requires chordino. Nature 387, 862–863.

Shibanuma, M., et al., 1993. Cloning from a mouse osteoblastic cell line of a set of transforming-growth-factor-beta 1-regulated genes, one of which seems to encode a follistatin-related polypeptide. Eur. J. Biochem. 217, 13–19.

Söllner, C., et al., 2003. Control of crystal size and lattice formation by starmaker in otolith biomineralization. Science 302, 282–286.

Solnica-Krezel, L., et al., 1996. Mutations affecting cell fates and cellular rearrangements during gastrulation in zebrafish. Development 123, 67–80.

Talbot, W.S., et al., 1995. A homeobox gene essential for zebrafish notochord development. Nature 378, 150–157.

Thisse, B., Thisse, C., 2004. Fast release clones: a high throughput expression analysis. Gene Expression Section (http://zfin.org).

Thisse, C., et al., 1994. goosecoid expression in neurectoderm and mesendoderm is disrupted in zebrafish cyclops gastrulas. Dev. Biol. 164, 420–429.

Thisse, B., et al., 2001. Expression of the zebrafish genome during embryogenesis. Gene expression section (http://zfin.org).

Thisse, B., et al., 2004. Spatial and temporal expression of the zebrafish genome by large-scale in situ hybridization screening. Methods Cell Biol. 77, 505–519.

Towers, P., et al., 1999. Flik, a chick follistatin-related gene, functions in gastrular dorsalisation/neural induction and in subsequent maintenance of midline Sonic hedgehog signalling. Dev. Biol. 214, 298–317.

Yabe, T., et al., 2003. Ogon/Secreted Frizzled functions as a negative feedback regulator of Bmp signaling. Development 130, 2705–2716.

Zimmerman, L.B., et al., 1996. The Spemann organizer signal noggin binds and inactivates bone morphogenetic protein 4. Cell 86, 599–606.